Constraints on the binary NS merger remnant and outflow structure from EM counterparts of GW170817

Ramandeep Gill
Open University of Israel

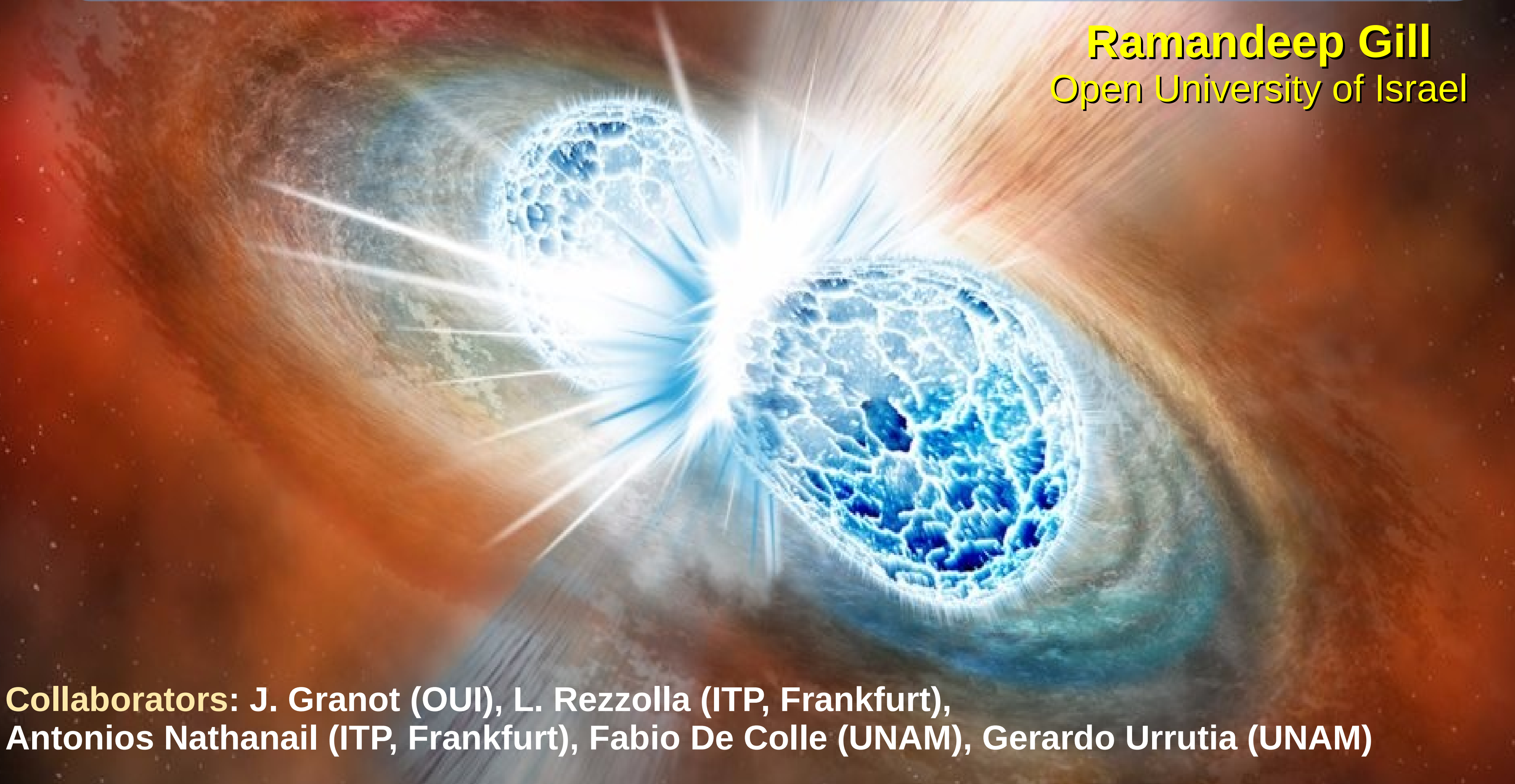

Collaborators: J. Granot (OUI), L. Rezzolla (ITP, Frankfurt), Antonios Nathanail (ITP, Frankfurt), Fabio De Colle (UNAM), Gerardo Urrutia (UNAM)

25 yrs of Konus-Wind: Ioffe Institute, St Petersburg Sept. 13, 2019

Some important questions

1. What do the **kilonova observations** and **delay between the GW chirp signal and prompt gamma-ray** onset tell us about the **merger remnant**?

2. **Can we still use initially top-hat jet simulations to model afterglows?**

3. Are there any **diagnostics** to **help understand the structure of the outflow** in future such events?

   a. **Flux-centroid motion**   b. **Image shape and size**   c. **Polarization**

BNS Merger Remnant

4 possible options

- Chirp mass from GW signal

$$\mathcal{M} \equiv (M_1 M_2)^{3/5}(M_1 + M_2)^{-1/5}$$
$$= 1.188^{+0.004}_{-0.002}\, M_\odot \qquad \text{(Abbott+17)}$$

(Granot, Guetta, & Gill 2017)

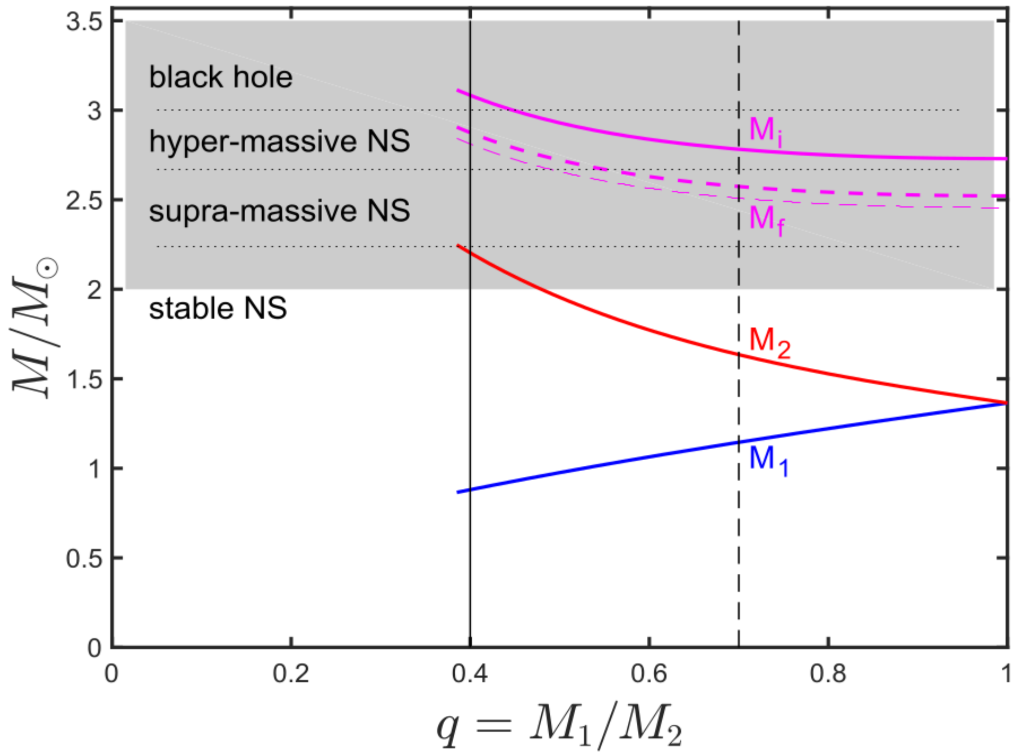

Maximum mass argument

- **GW 170817:** $M_{\rm tot} = 2.74^{+0.04}_{-0.01} M_\odot$

- Threshold for direct collapse to BH

$$M_{\rm th} \approx 1.415 M_{\rm TOV} \approx 2.82 M_\odot$$

(Bauswein+13, 17; Koppel+19)

- Max. mass supported by uniform rotation

$$M_{\rm max} = (1.20 \pm 0.02) M_{\rm TOV} \simeq 2.40 M_\odot$$

(Breu & Rezzolla ‘16)

- Max. mass supported by differential rotation

$$M_{\rm max,dr} \simeq (1.54 \pm 0.05) M_{\rm TOV} \simeq 3.08 M_\odot$$

(Weih+18)

Assuming: $M_{\rm TOV} = 2 M_\odot$

Can it be a supra-massive magnetar?

- Supported by rigid-body rotation and collapses to a BH on the spin-down time.

$$\tau_{\rm sd} = \frac{Ic^3}{2f\Omega_0^2 R_{\rm NS}^6 B_0^2} \gtrsim 3.4\times10^4 \frac{P_{0,-3}^2}{fB_{14}^2}\ {\rm s} \qquad E_{\rm rot} = \frac{1}{2}I\Omega_0^2 \sim 10^{52.5} - 10^{53}\ {\rm erg}$$

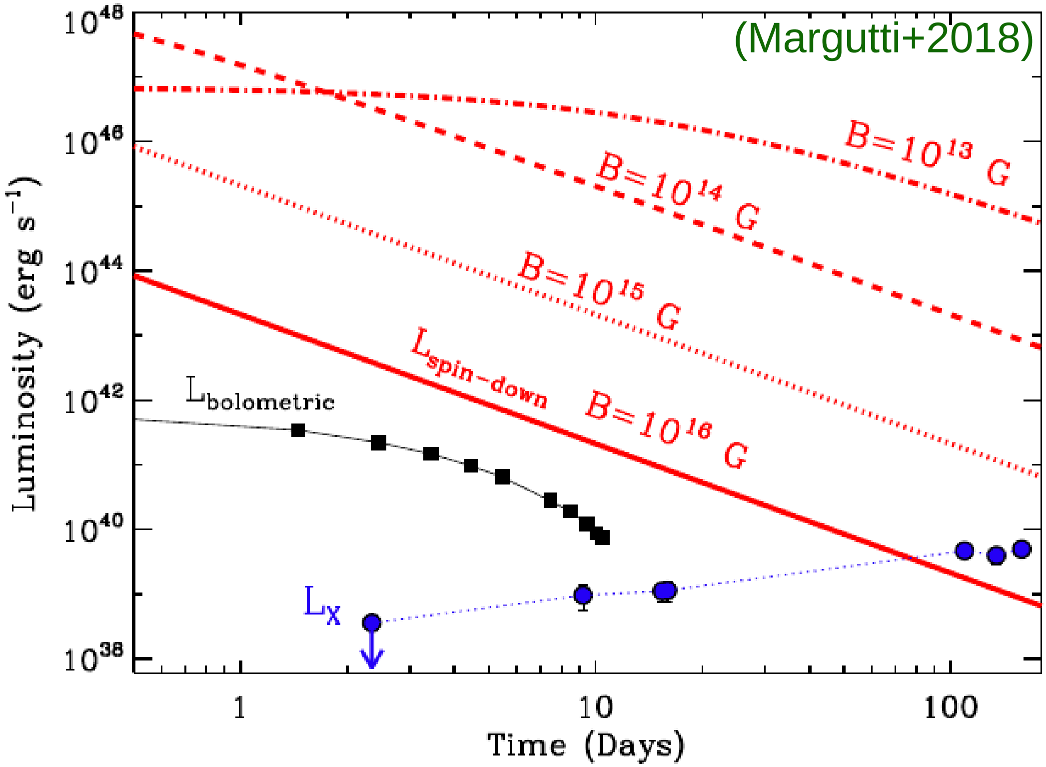

- Energy injected by the spinning down NS in the form of an isotropic pulsar-type MHD wind would've powered an exceptionally bright afterglow.

- Early afterglow observations ruled out a supra-massive NS
  (e.g. Granot+17; Margalit & Metzger '17; Pooley+18)

Hypermassive NS (HMNS) and mass ejection

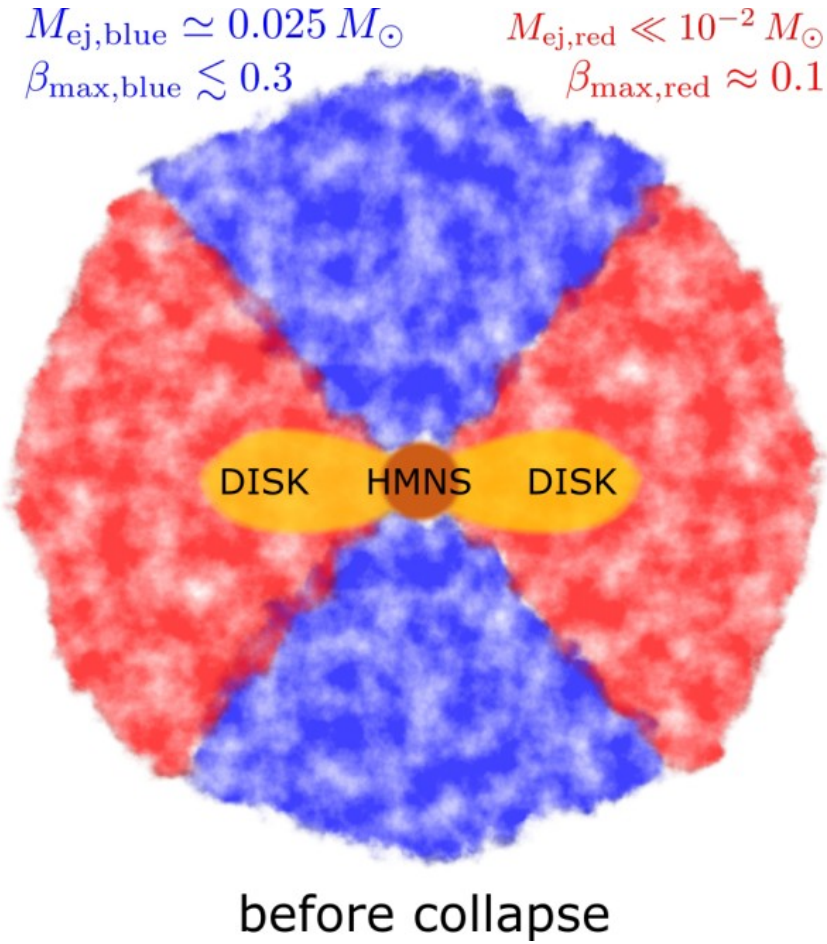

(Gill, Nathanail, Rezzolla, '19; Kasen+17)

(Kasen+17)

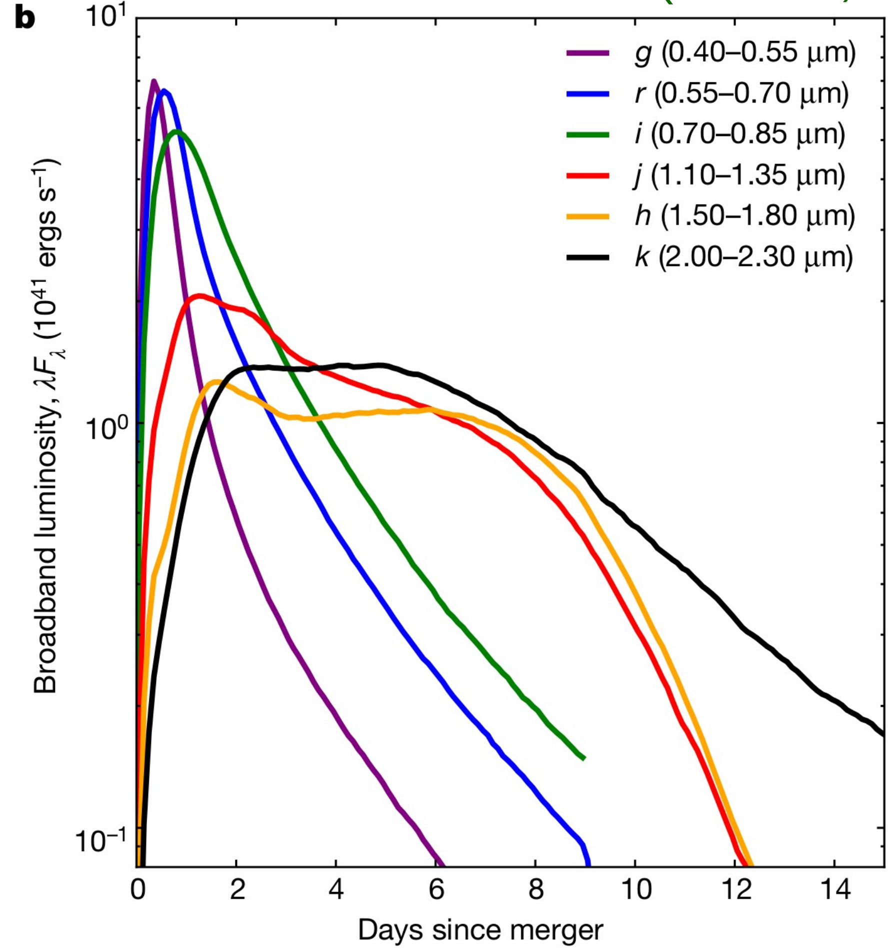

(Kilonova observation: Arcavi et al. 2017; Cowperthwaite et al. 2017; Drout et al. 2017; Evans et al. 2017; Kasliwal et al. 2017; Kilpatrick et al. 2017; Pian et al. 2017; Shappee et al. 2017; Smartt et al. 2017; Troja et al. 2017; ...)

Different mass ejection channels and their rates

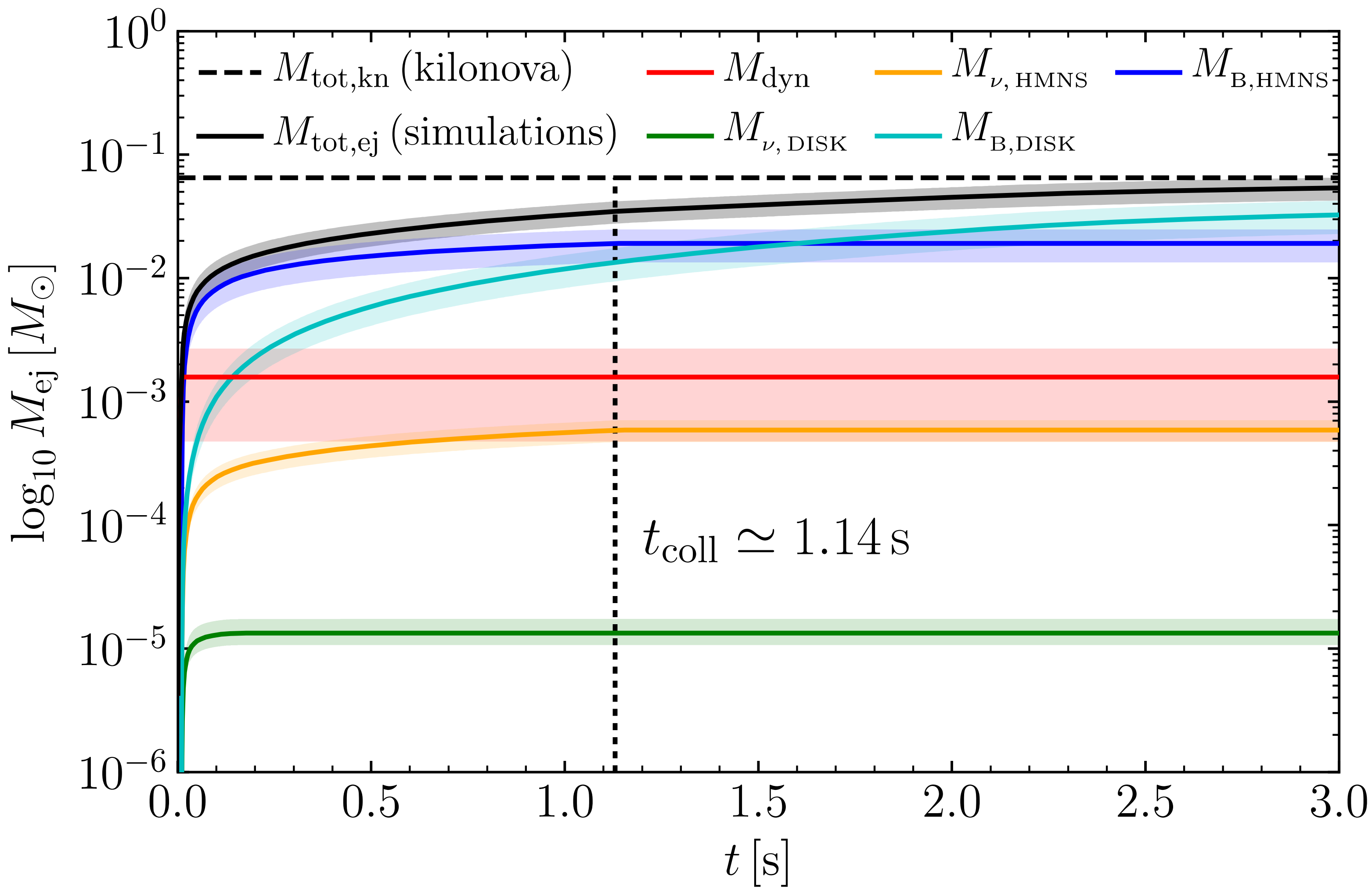

(Gill, Nathanail, Rezzolla , 2019)

HMNS collapse time limit from blue ejecta mass

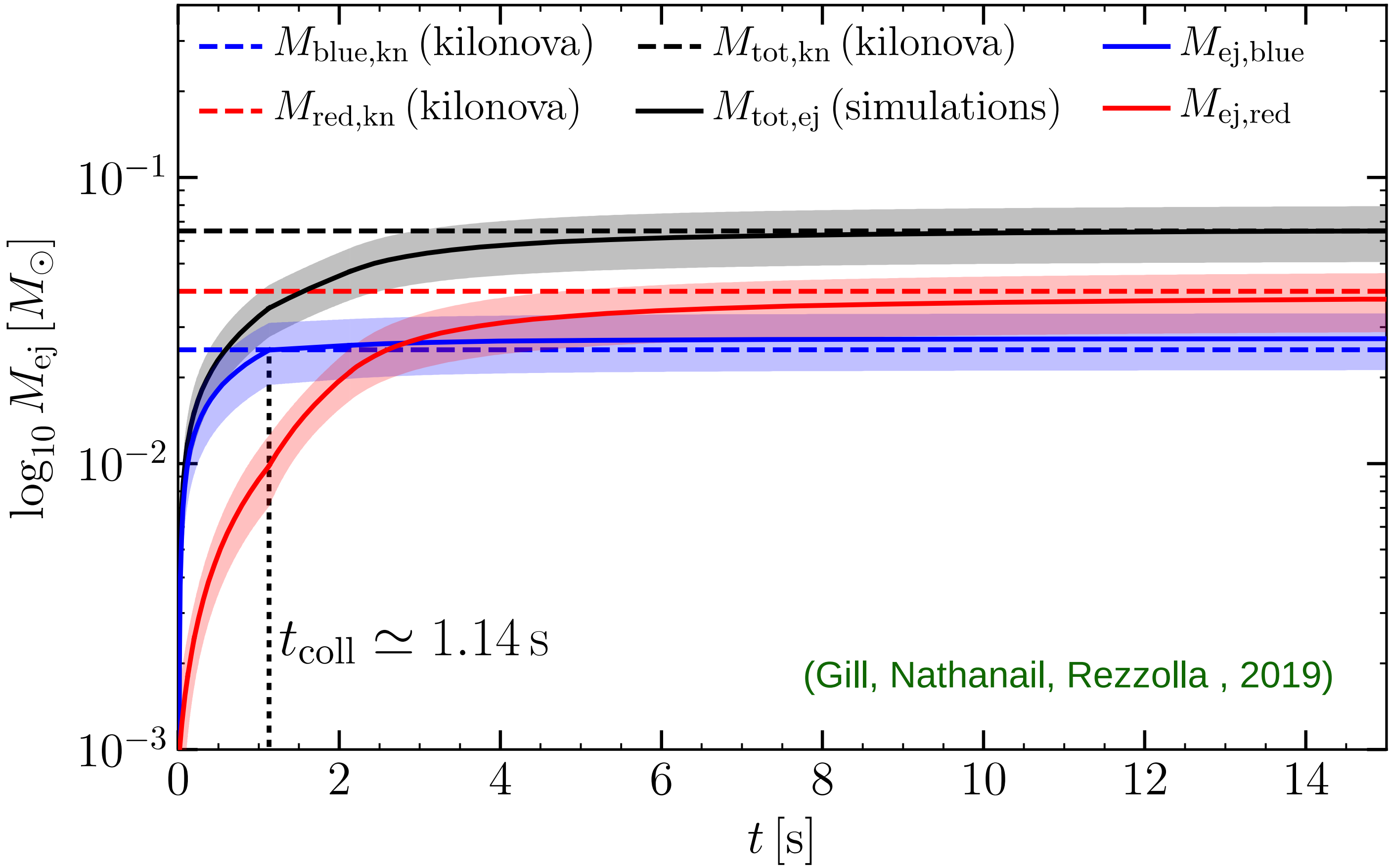

Collapse time of HMNS: $t_{\rm coll} = 1.14^{+0.60}_{-0.50}\ {\rm s}$

(also see, e.g., Granot+17; Metzger+18)

The delayed GRB onset

- Temporal delay between GW chirp signal and SGRB onset:

$$t_{\rm del} = 1.74 \pm 0.05 \text{ s}$$

(LVC+Fermi+INTEGRAL 2017)

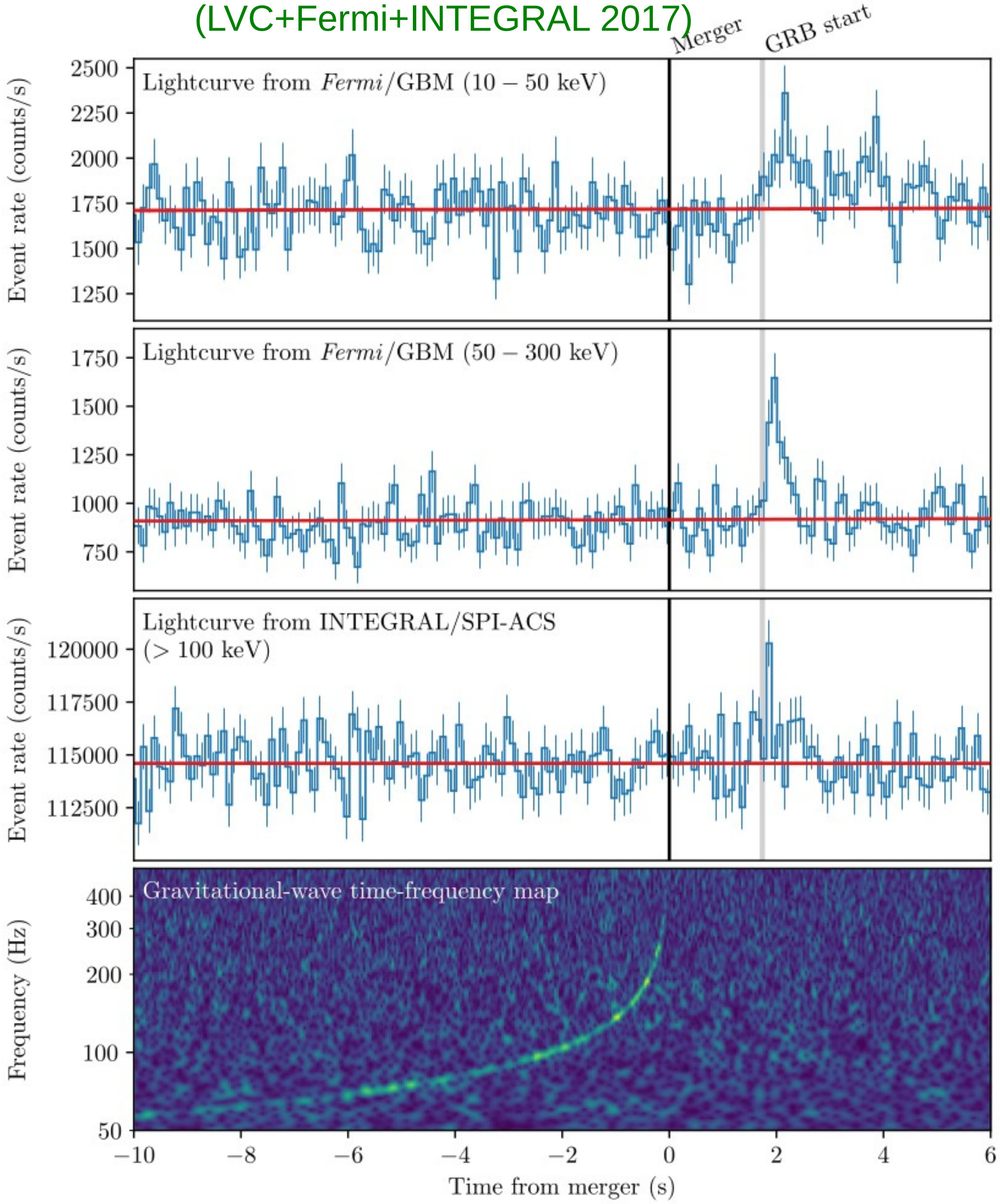

The delayed GRB onset

- Temporal delay between GW chirp signal and SGRB onset:

$$t_{\rm del} = 1.74 \pm 0.05 \text{ s}$$

- The delay time is a combination of **three timescales**:

$$t_{\rm del} = t_{\rm coll} + t_{\rm br}(t_{\rm coll}) + t_R$$

$$t_R = \frac{R_\gamma}{2\Gamma^2 c} = 0.5 \left(\frac{R_\gamma}{7.5 \times 10^{11} \text{ cm}} \right) \left(\frac{\Gamma}{5} \right)^{-2} \text{ s}$$

$\Gamma \gtrsim 5$ (from pair opacity - Matsumoto+19)

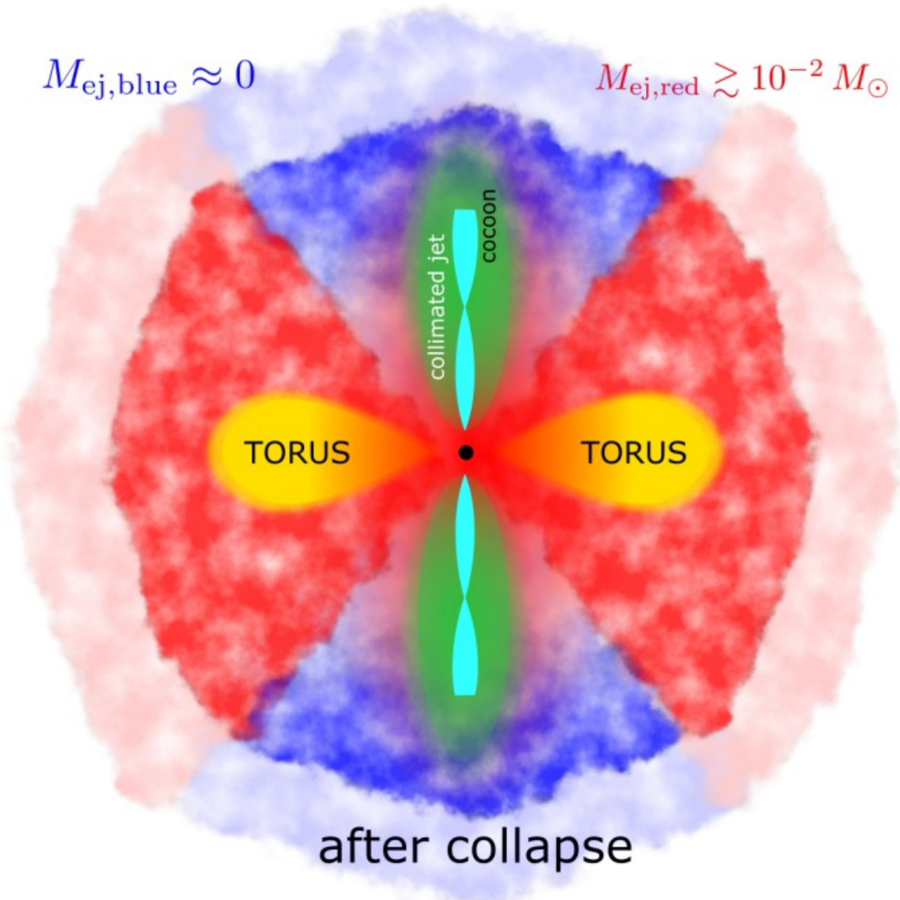

(Gill, Nathanail, Rezzolla , 2019)

The delayed GRB onset

- Temporal delay between GW chirp signal and SGRB onset:

$$t_{\rm del} = 1.74 \pm 0.05 \text{ s}$$

- The delay time is a combination of **three timescales**:

$$t_{\rm del} = t_{\rm coll} + t_{\rm br}(t_{\rm coll}) + t_R$$

$$t_R = \frac{R_\gamma}{2\Gamma^2 c} = 0.5 \left(\frac{R_\gamma}{7.5\times10^{11}\ \text{cm}}\right)\left(\frac{\Gamma}{5}\right)^{-2} \text{ s}$$

$\Gamma \gtrsim 5$ (from pair opacity - Matsumoto+19)

- Jet breakout time depends on the properties of the jet and circum-merger **(homologously expanding) ejecta**:

$$\rho_{\rm ej}(r<R_{\rm ej},t) \propto \frac{M_{\rm ej,blue}(t)}{R_{\rm ej}^3(t)}\left[\frac{r}{R_{\rm ej}(t)}\right]^{-k}$$

$$R_{\rm ej}(t) = \beta_{\max} c t$$

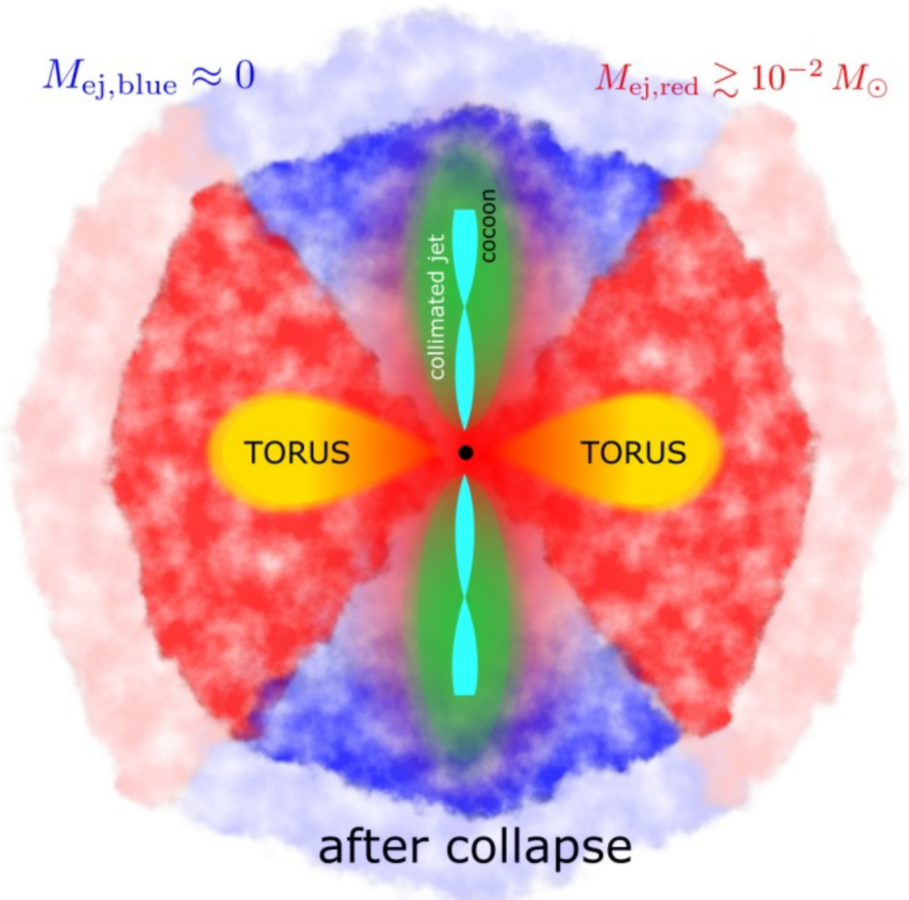

(Gill, Nathanail, Rezzolla , 2019)

The delayed GRB onset

- Temporal delay between GW chirp signal and SGRB onset:

$$t_{\rm del} = 1.74 \pm 0.05 \text{ s}$$

- The delay time is a combination of **three timescales**:

$$t_{\rm del} = t_{\rm coll} + t_{\rm br}(t_{\rm coll}) + t_R$$

$$t_R = \frac{R_\gamma}{2\Gamma^2 c} = 0.5 \left(\frac{R_\gamma}{7.5 \times 10^{11} \text{ cm}} \right) \left(\frac{\Gamma}{5} \right)^{-2} \text{ s}$$

$\Gamma \gtrsim 5$ (from pair opacity - Matsumoto+19)

- Jet breakout time depends on the properties of the jet and circum-merger **(homologously expanding) ejecta**:

$$\rho_{\rm ej}(r < R_{\rm ej}, t) \propto \frac{M_{\rm ej,blue}(t)}{R_{\rm ej}^3(t)} \left[\frac{r}{R_{\rm ej}(t)} \right]^{-k}$$

$$R_{\rm ej}(t) = \beta_{\max} c t$$

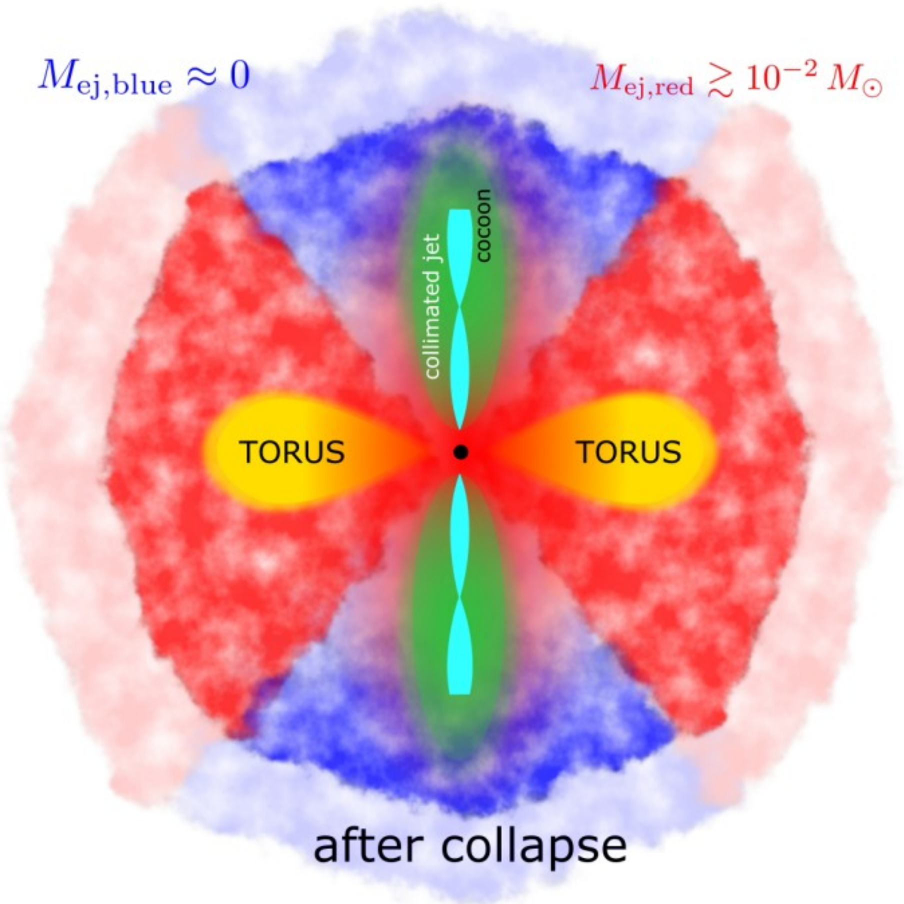

(Gill, Nathanail, Rezzolla , 2019)

- We inject a uniform jet and use the semi-analytic model of Bromberg+11 to calculate its breakout time.

HMNS collapse time from delayed GRB onset

(Gill, Nathanail, Rezzolla , 2019)

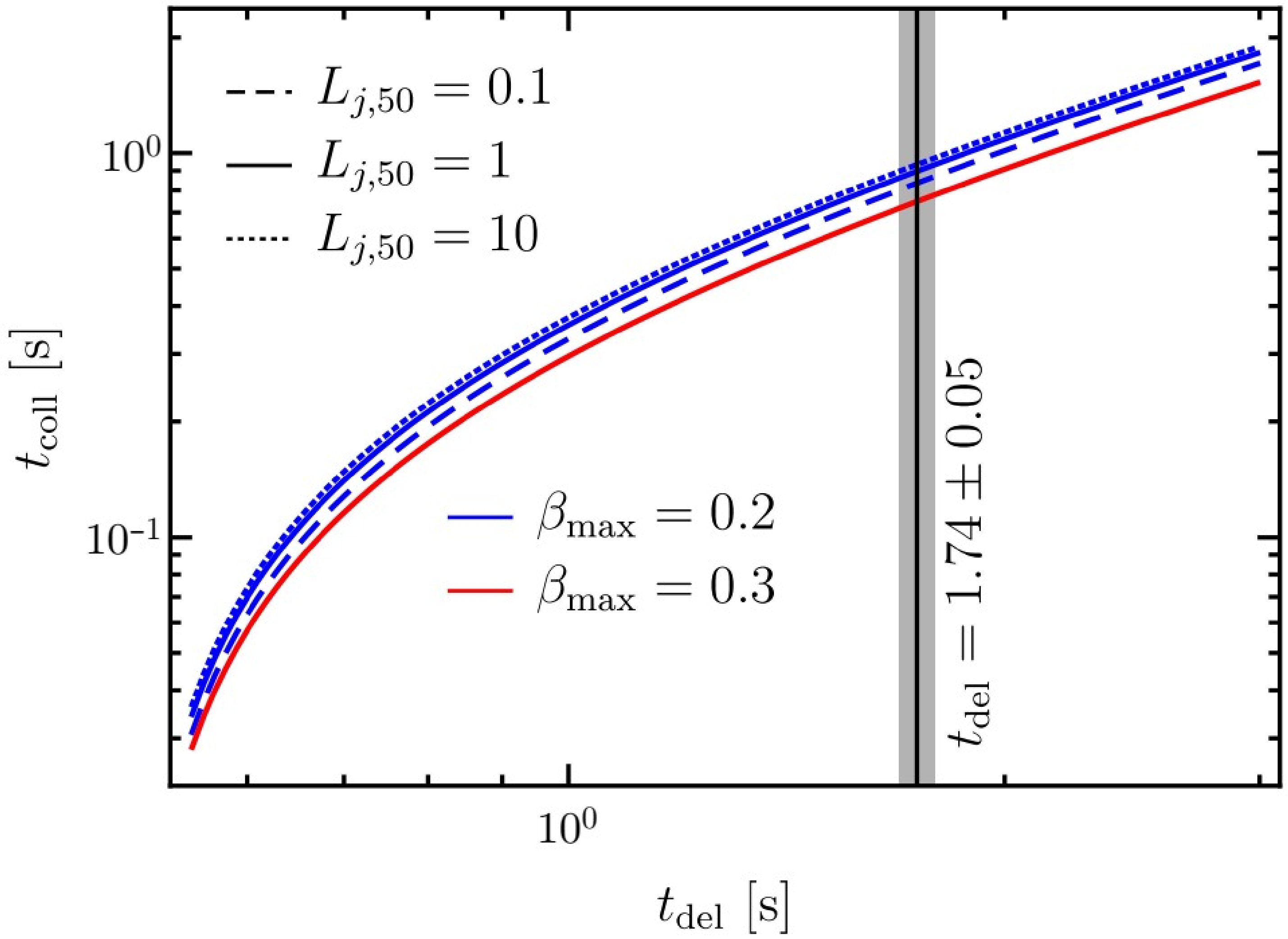

$$\boxed{t_{\rm coll} = 0.82 \pm 0.15 \text{ s}}$$

HMNS collapse time

(Gill, Nathanail, Rezzolla , 2019)

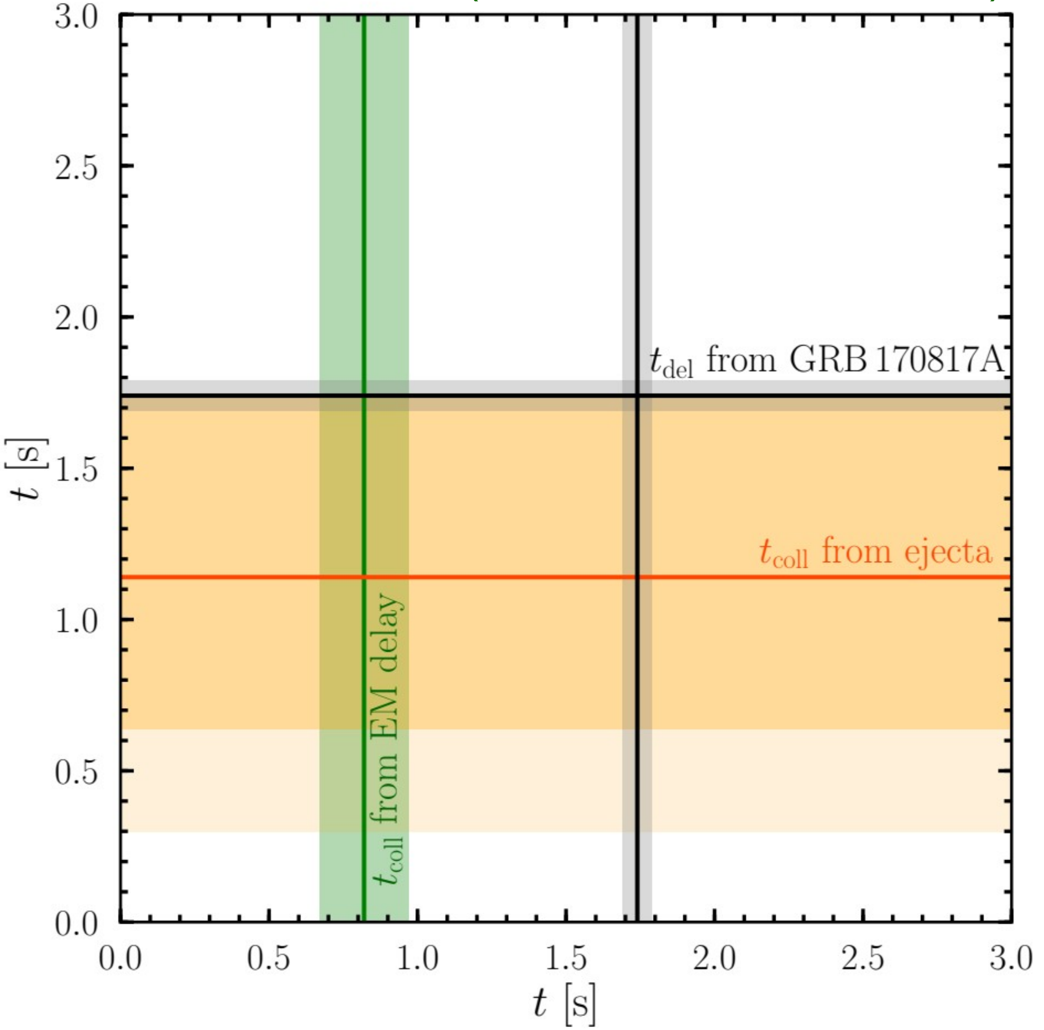

$$t_{\rm coll} = 0.98^{+0.31}_{-0.26}\ \rm s$$

Afterglow Emission

Long lasting rise of the afterglow

$$S_\nu \propto \nu^{-0.6} t^{0.8}$$

(Mooley+2017)

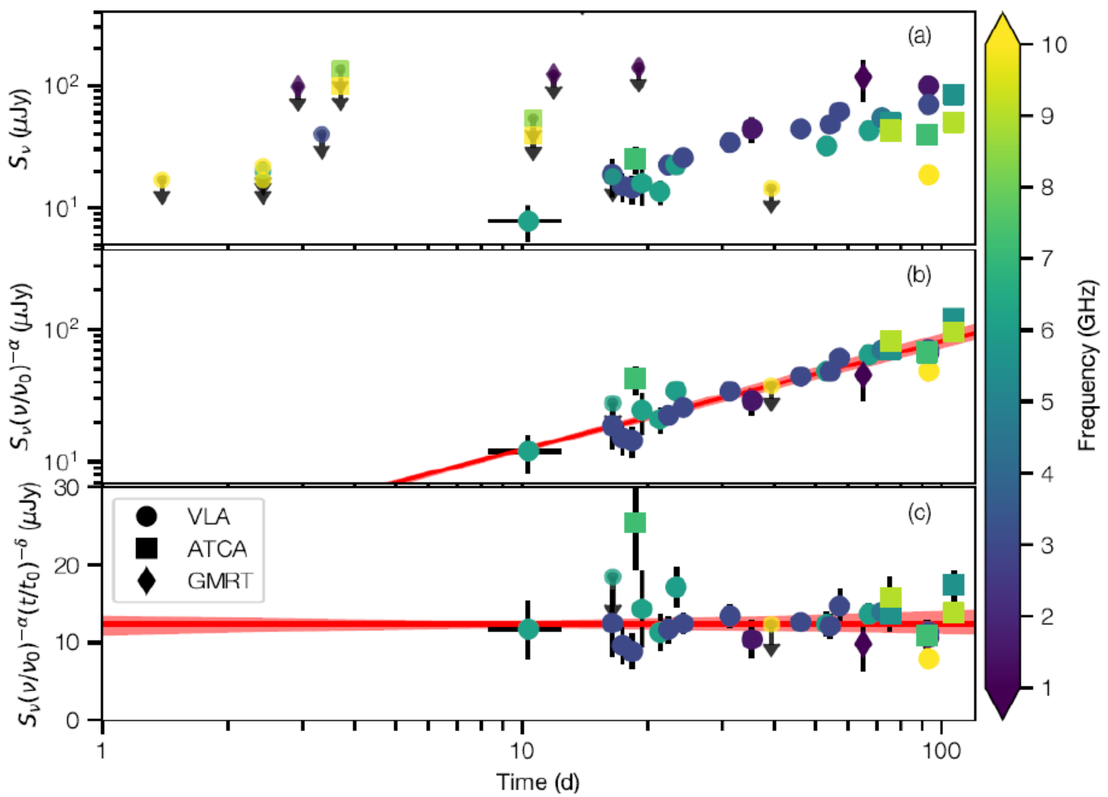

(Margutti+2018)

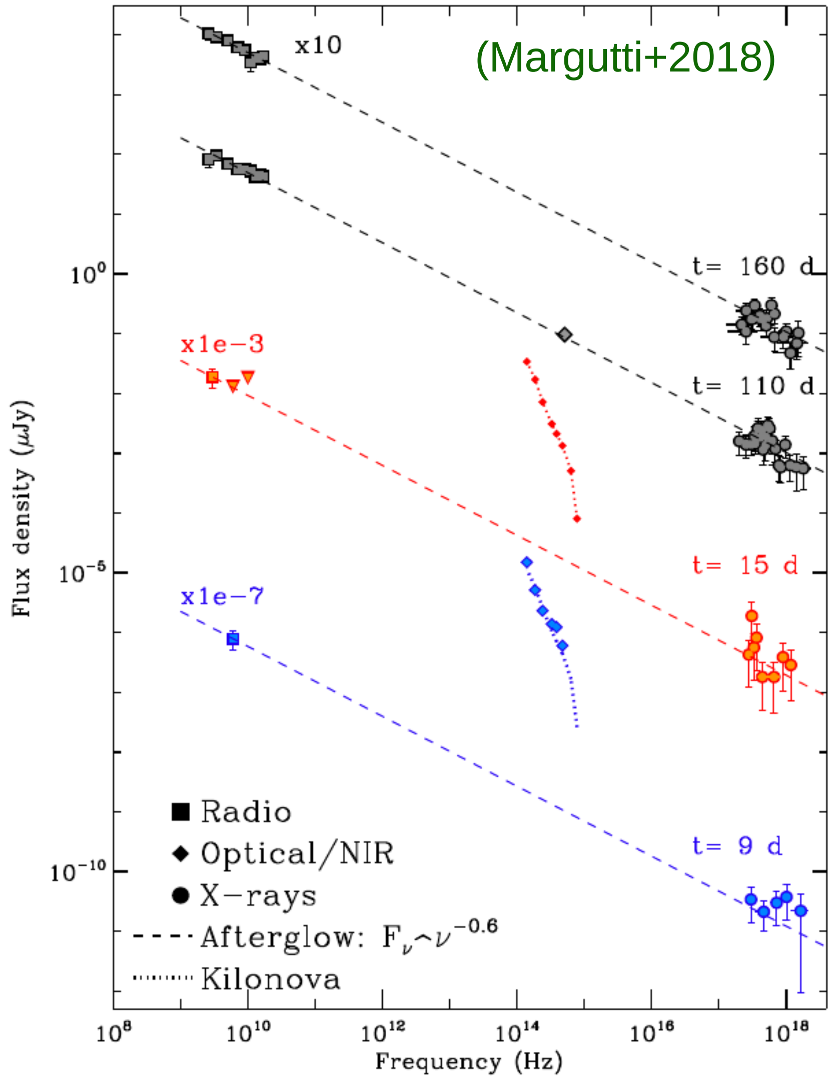

Failure of the **initially** top-hat jet model – but wait!

- The initially top-hat jet model failed at explaining the data at early times (e.g., Margutti+18; Mooley+18)
- At early times, the model lightcurve rose much sharply as compared to a shallower rise of the flux.

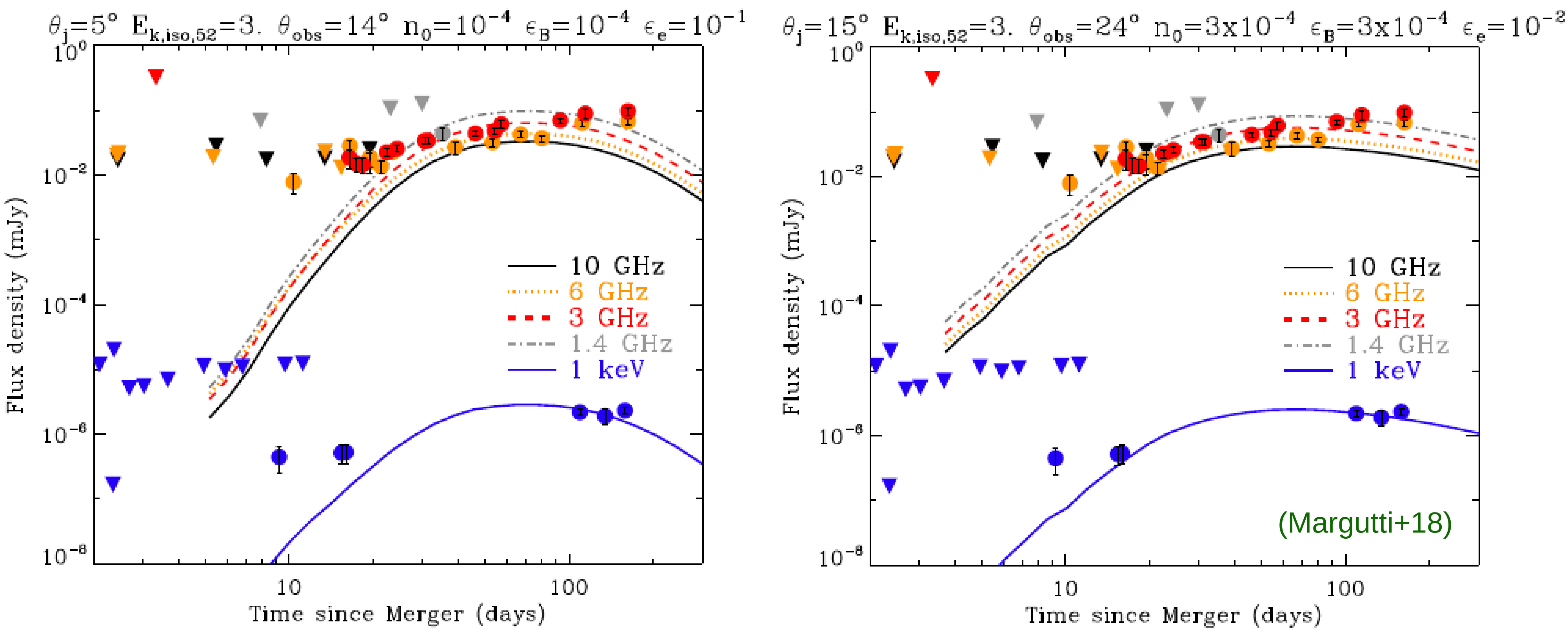

Initially top-hat jet numerical simulation

- We conducted 2D hydro simulations of an initially top-hat jet with Blandford-McKee (1976) self-similar dynamics and derived the afterglow lightcurves by post-processing.

(Gill, Granot, De Colle, Urrutia, 2019)

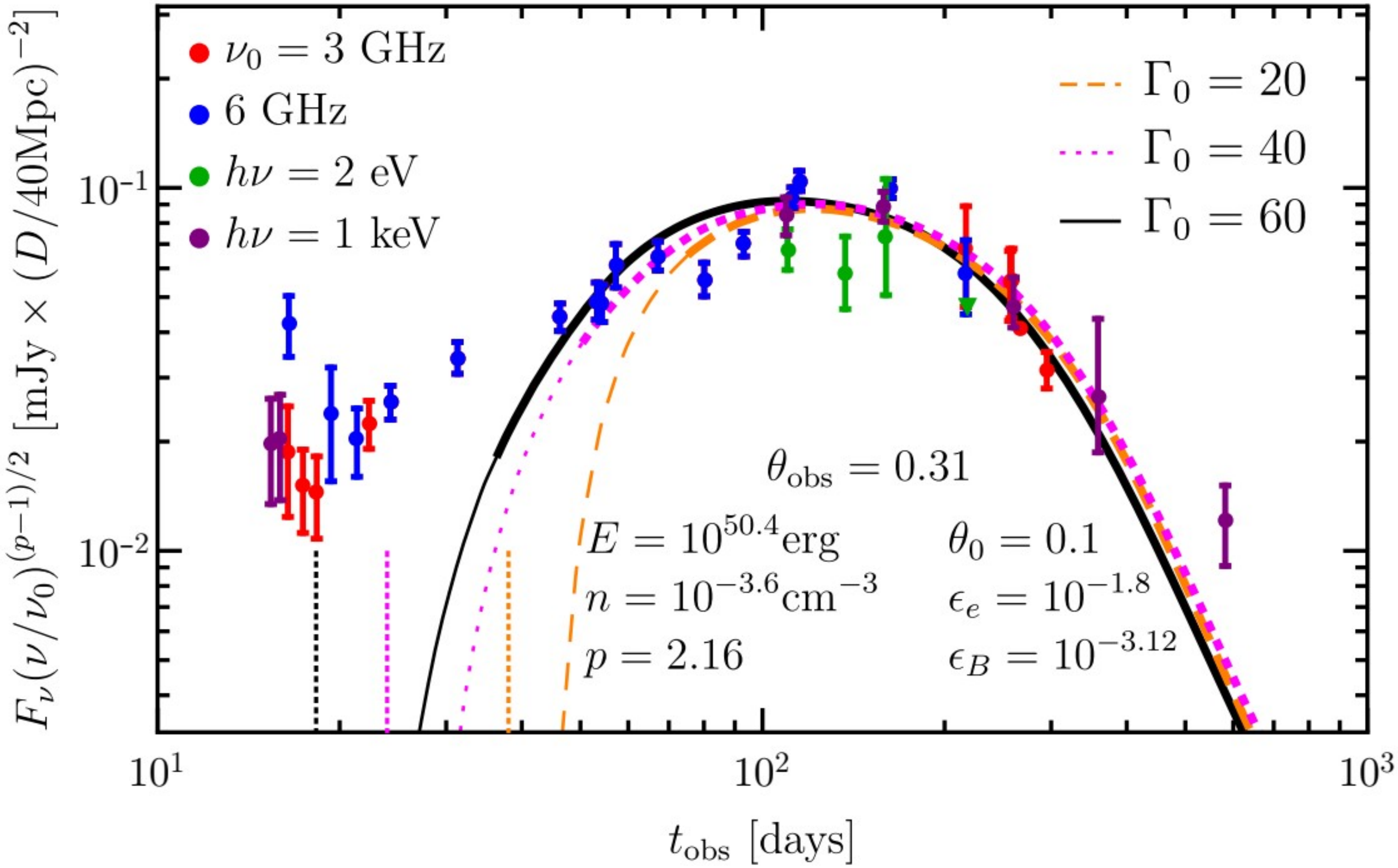

Angular time delay: $\frac{t_{\mathrm{obs},\theta}}{(1+z)} = \frac{R_0}{c}[1-\cos(\Delta\theta)] \approx \frac{\Delta\theta^2}{2} t_0 \propto \Gamma_0^{-2/(3-k)}$

Off-axis emission from a structured jet

- Simulation of a jet emerging from non-relativistic NS-NS merger ejecta, giving the jet angular structure (Lazzati+18).
- Also see: Margutti+18; Xie+18

(Lazzati+18)

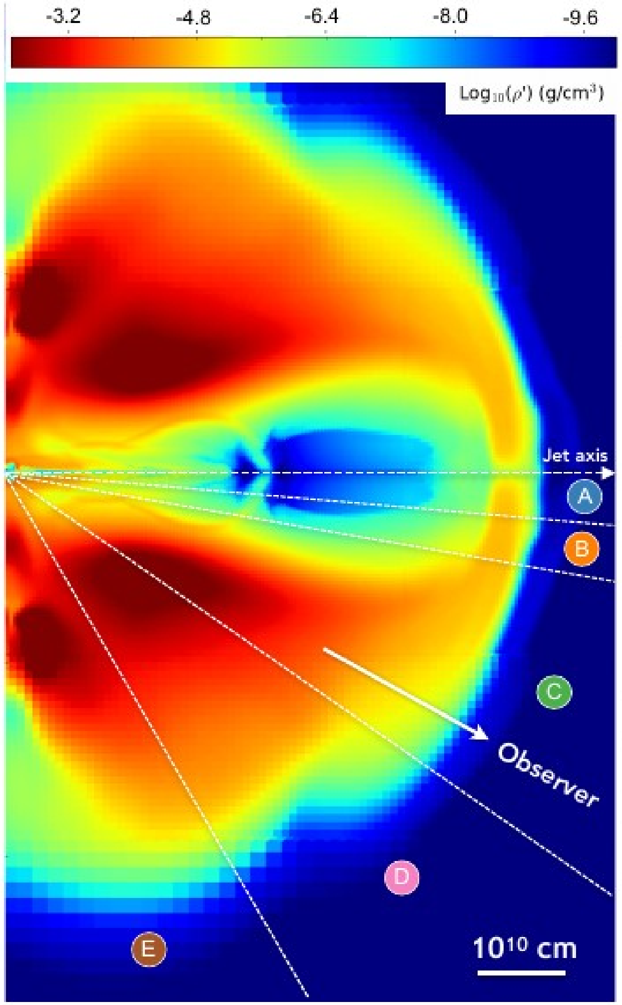

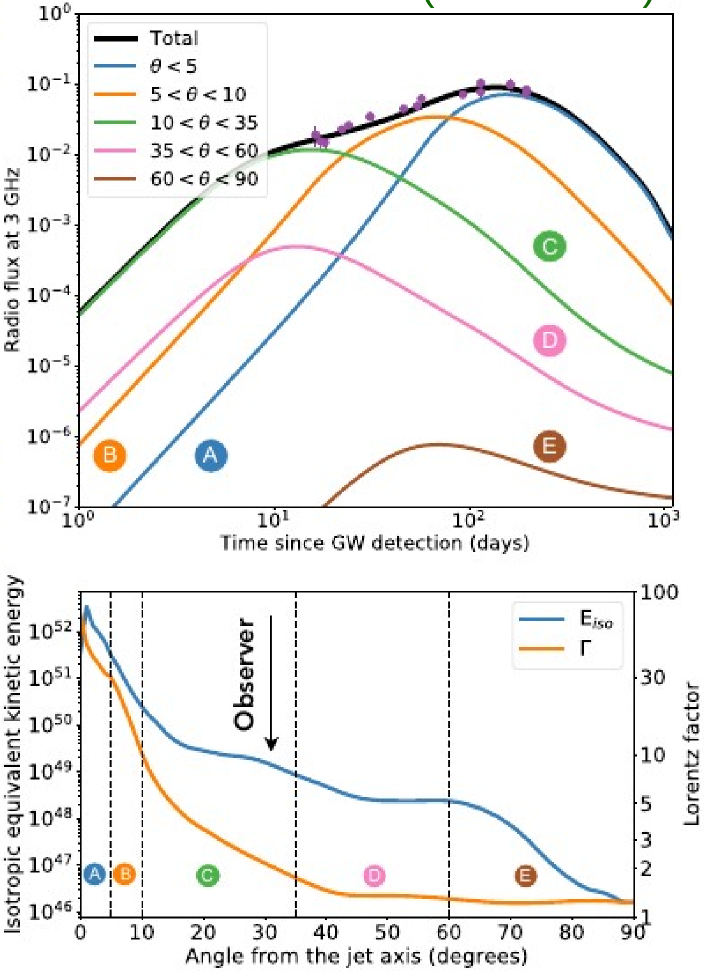

Four diagnostics of outflow structure

Semi-analytic lightcurves from structured jets / cocoons

(Gill & Granot 18)

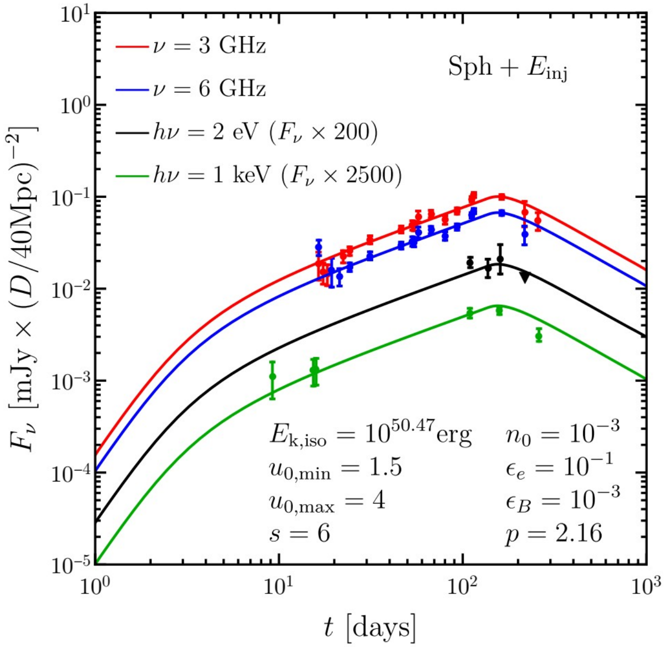

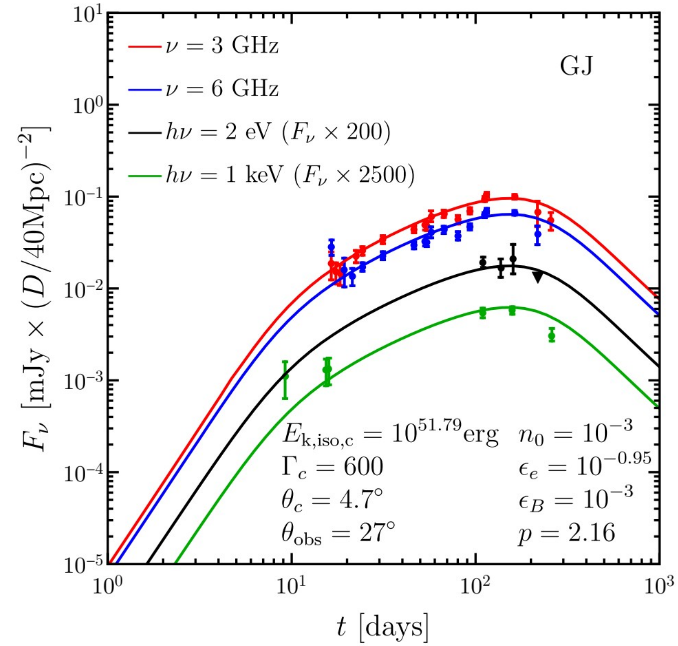

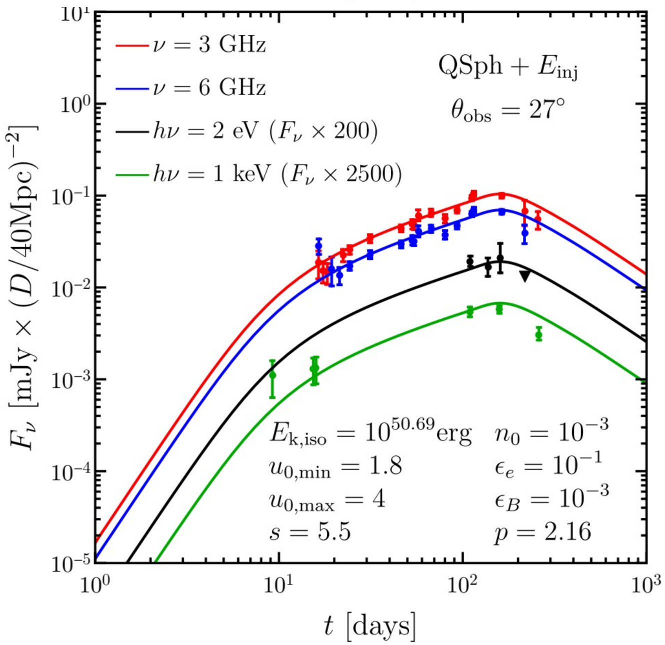

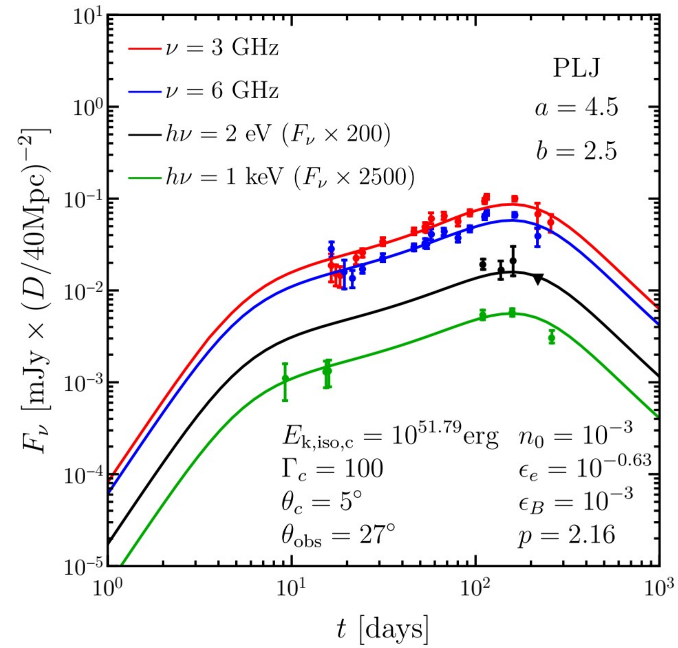

Also see: Lamb & Kobayashi 18; Troja+18; Fraija & Veres+18; D'Avanzo+18; Troja+17,18; Resmi+18

Afterglow images

- Important properties of the outflow can be derived from afterglow images.
- $\theta_{\rm obs} = 27^\circ$; assumes local spherical dynamics (no lateral spreading).

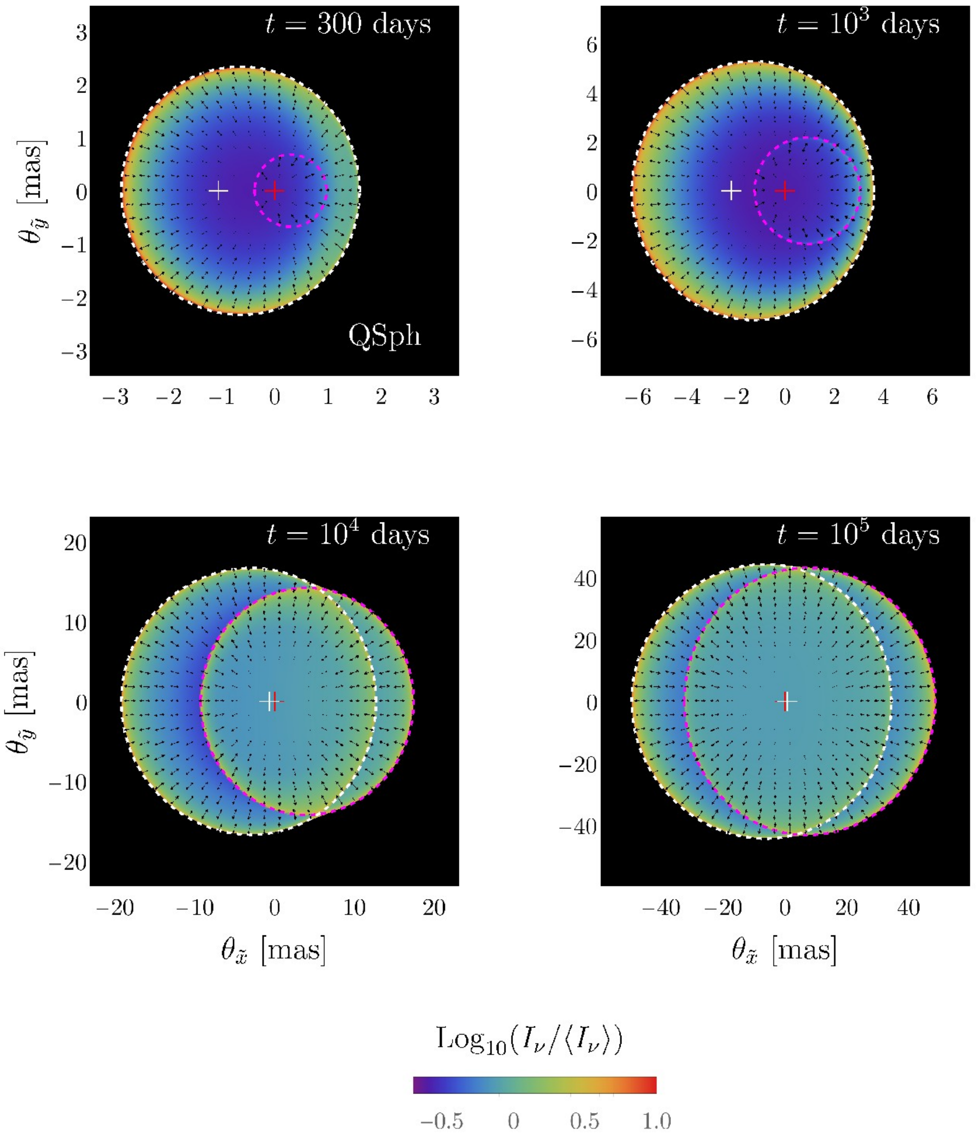

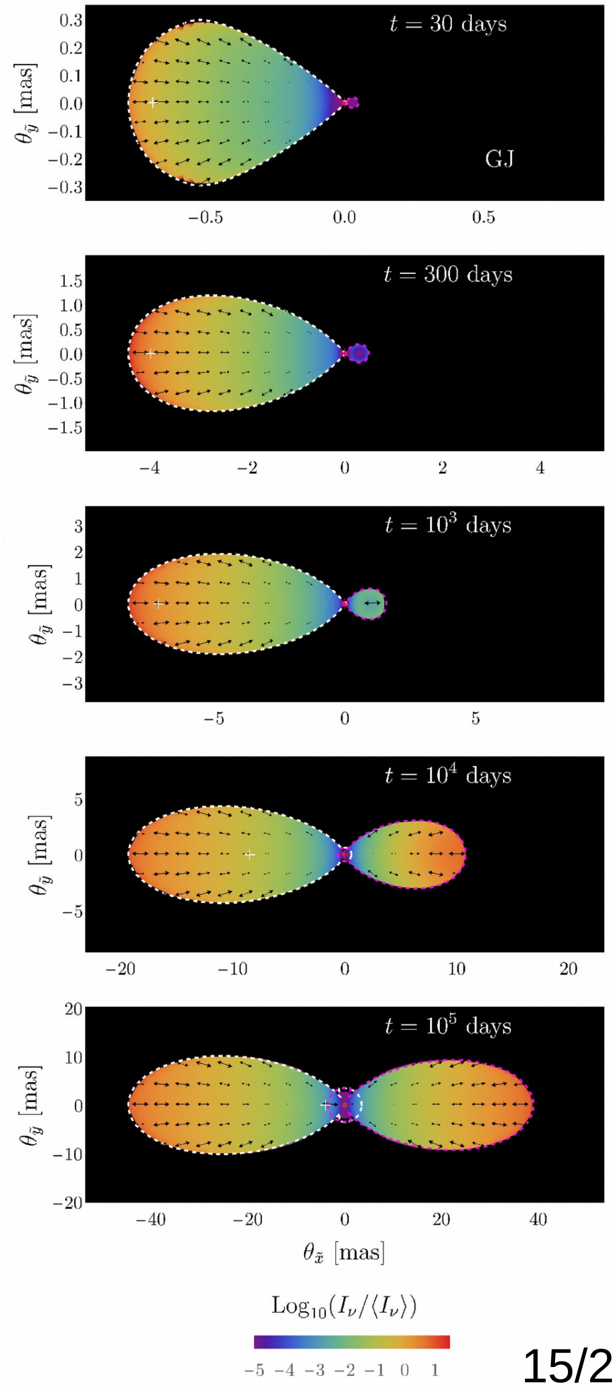

(Gill & Granot 18)

Postshock magnetic field structure

- Theoretical and numerical works find that magnetic fields are generated by the two-stream / Weibel instability at the collisionless relativistic afterglow shock (Gruzinov & Waxman '99, Medvedev & Loeb '99, Silva+03, Frederiksen+04, ..)

(Sironi, Keshet, Lemoine, 2015)

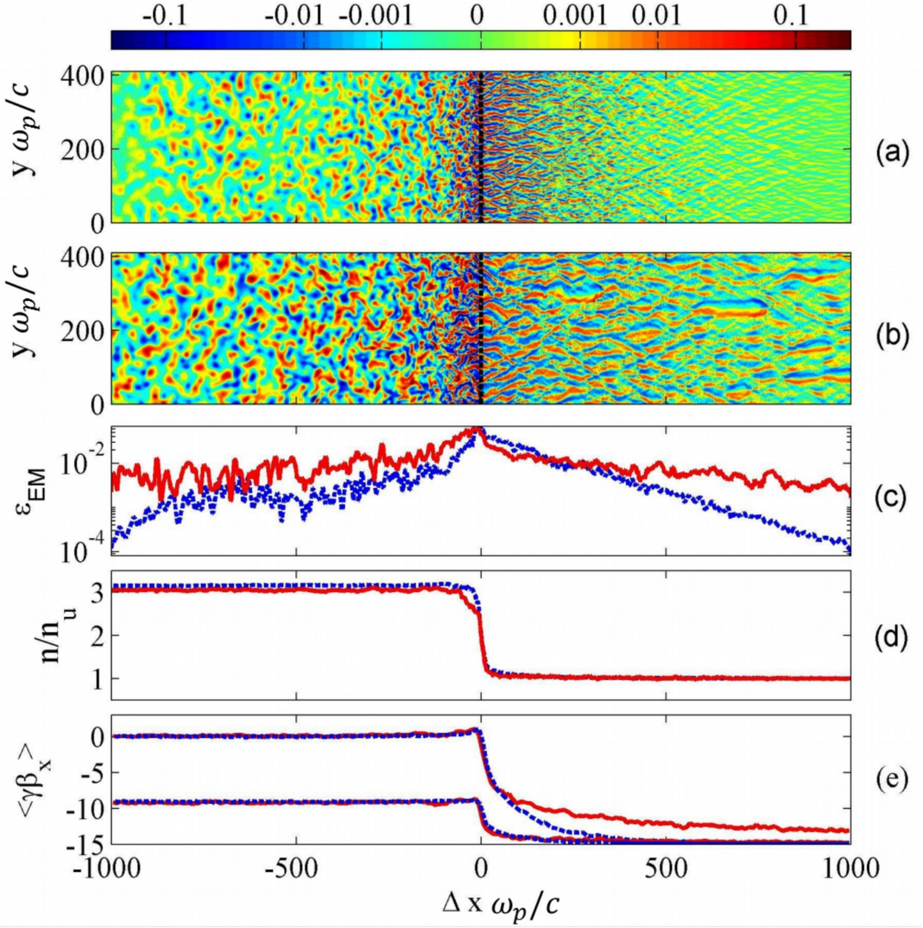

- The generated field is randomly oriented in the plane transverse to the shock normal.

- Its coherence scale is much smaller than the width of the shock:

$$\lambda_e = c/\omega_p \sim 2.3 \times 10^7 n_0^{-1/2}\,\mathrm{cm}$$

$$\ll \Delta'_{\rm sh} \sim R/\Gamma_{\rm sh} \sim 10^{14} R_{15} \Gamma_{\rm sh,1}^{-1}\,\mathrm{cm}$$

- In general, postshock field can be anisotropic

$$b = \frac{2\langle B_\parallel^2 \rangle}{\langle B_\perp^2 \rangle}$$

- Many works use volume averaged value for b=0 and assume an infinitely thin shell.

Polarization from random B-field

(Gill & Granot 18)

- Linear polarization can distinguish between outflow structure and provide insight into magnetic field structure.

- Assume random B field:

$$b = \frac{2\langle B_{\parallel}^2\rangle}{\langle B_{\perp}^2\rangle}$$

and infinitely thin shell geometry

- Upper limit on linear polarization (Corsi+18)

$$\Pi \lesssim 12\% \ (99\% \text{ C. L.})$$

show that for a structured jet

$$0.7 \lesssim b \lesssim 1.5$$

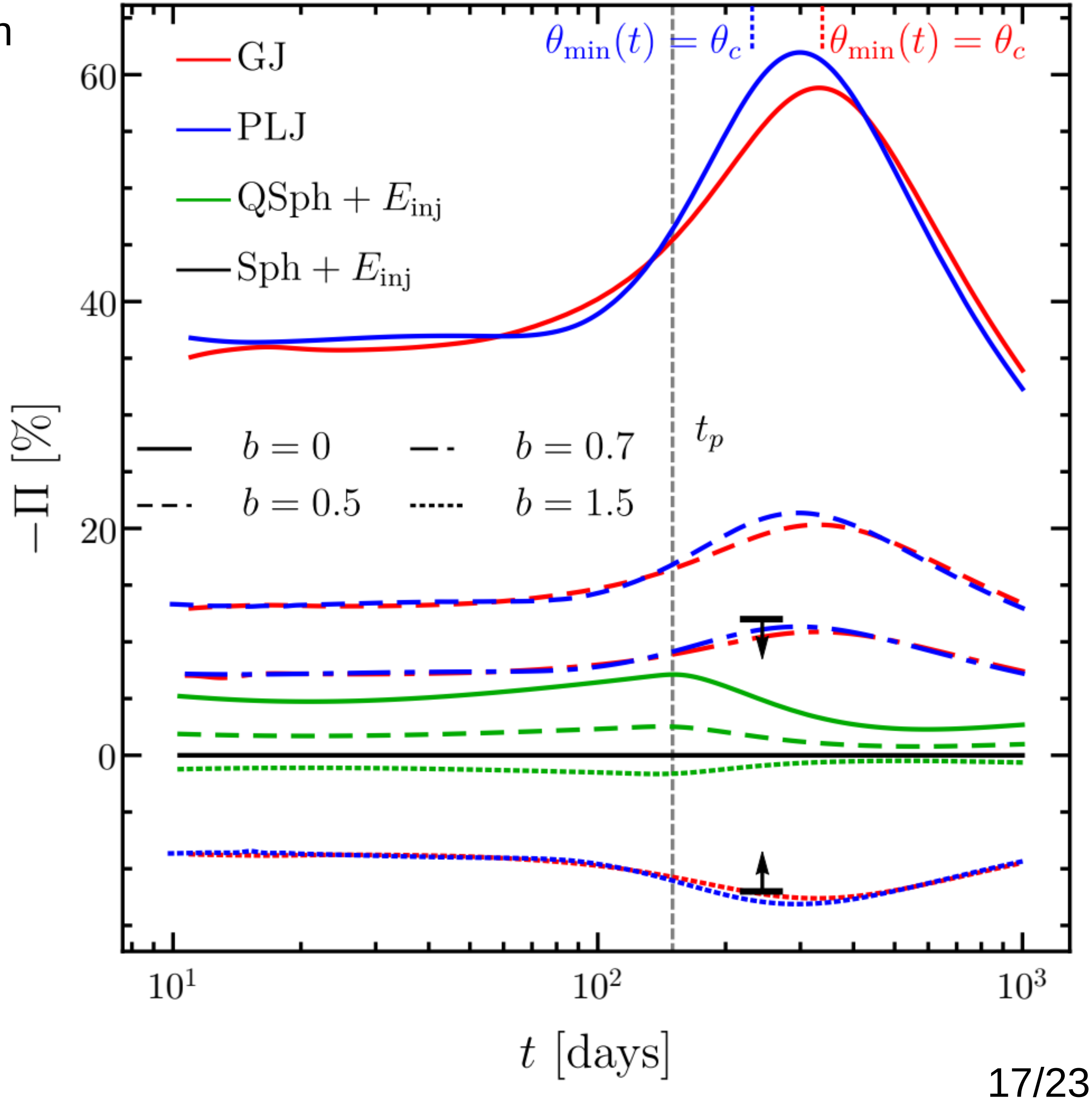

Radial structure of postshock magnetic field

- Assuming the "frozen field" approximation, the radial structure of the magnetic field is (Granot+99):

$$B_{\parallel}(\chi) = B_{\parallel,f}\,\chi^{-1/(8-2k)} \qquad B_{\perp} = B_{\perp,f}\,\chi^{-1} \qquad \chi = 1 + 2(4-k)\Gamma_{\rm sh}^2\left(\frac{R-r}{R}\right)$$

(Similarity variable)

- Downstream of the shock, the magnetic field becomes more radial:

$$\xi(\chi) = \frac{B_{\parallel}(\chi)}{B_{\perp}(\xi)} = \xi_f\,\chi^{(7-2k)/(8-2k)}$$ (Field anisotropy)

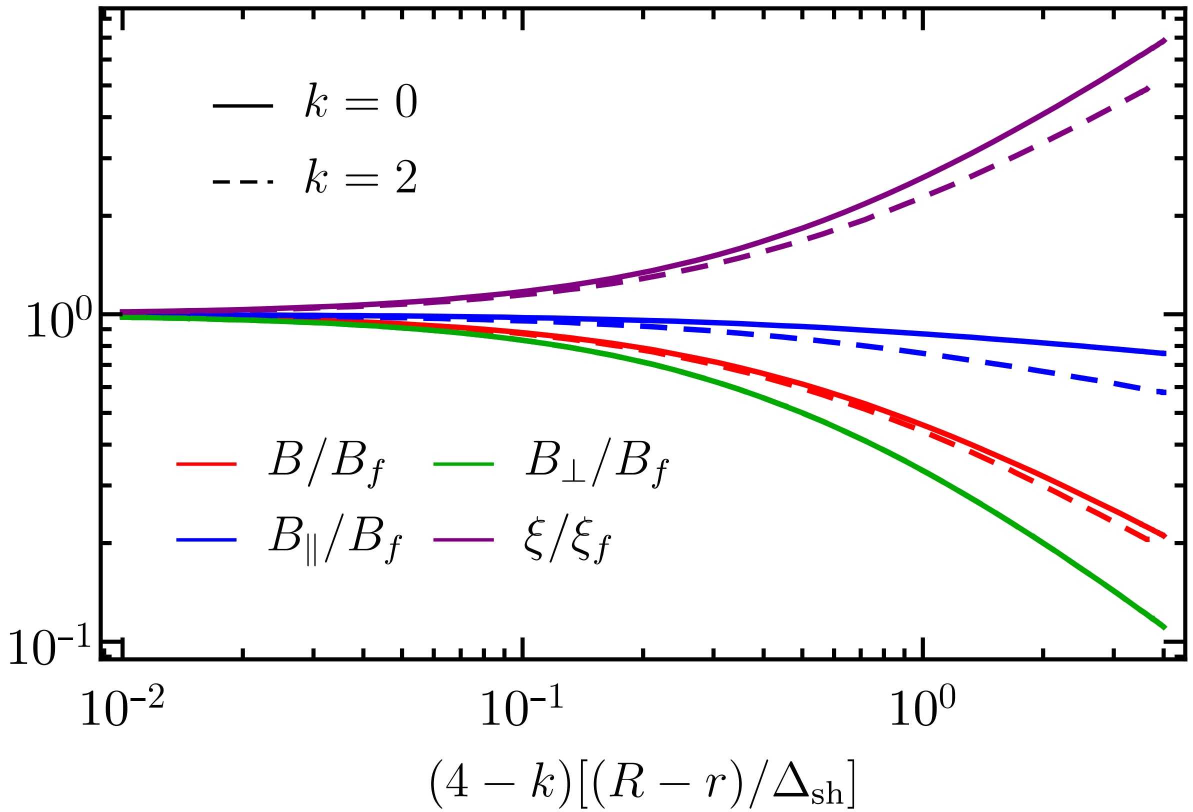

Polarization from volume integration of shocked region

- We integrate over the shocked volume and assume a “frozen-field” approximation
- The field anisotropy just behind the shock is parameterized with ξ_f

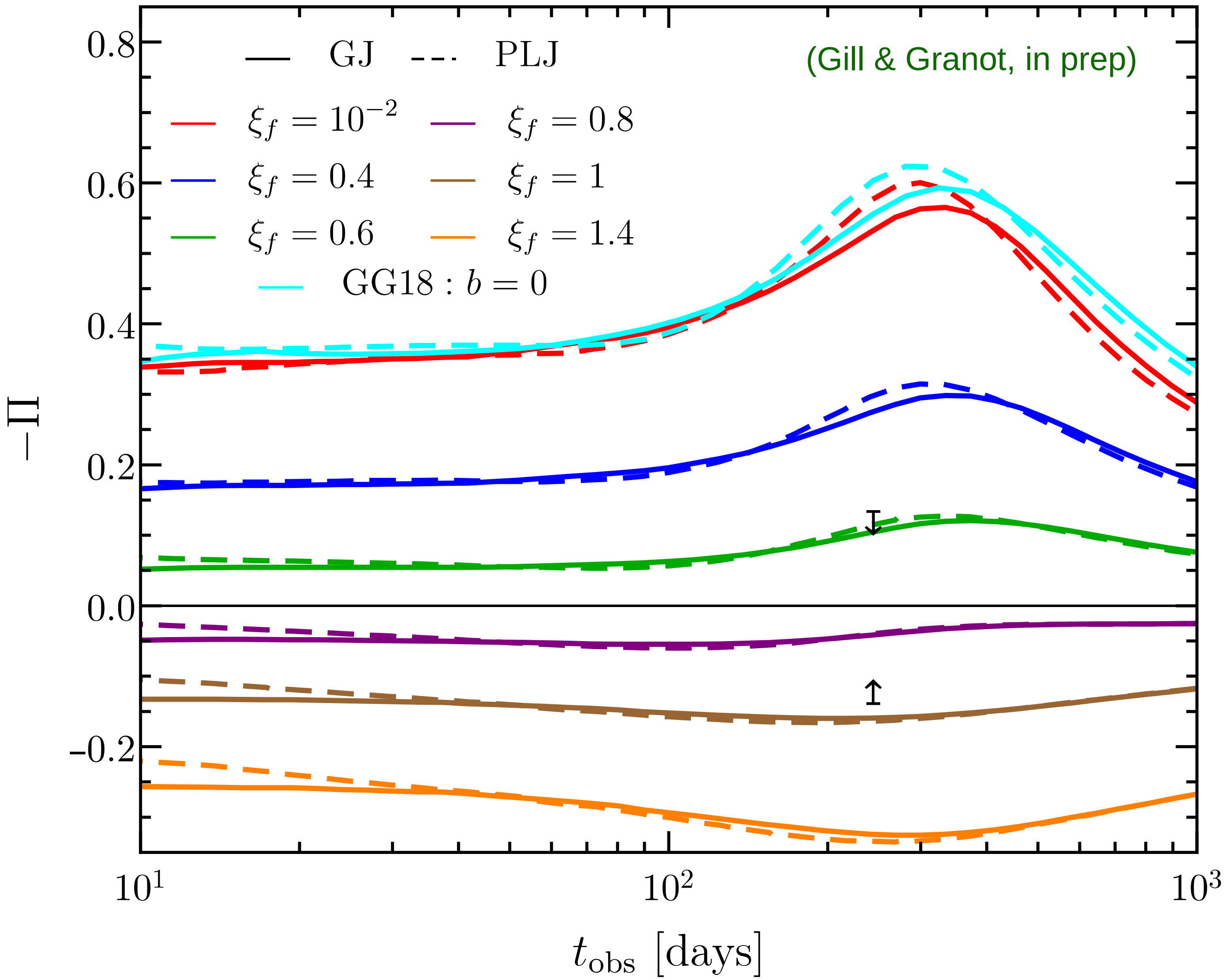

Comparison between 2D and 3D integration

- We integrate over the shocked volume and assume a “frozen-field” approximation
- The field anisotropy just behind the shock is parameterized with ξ_f

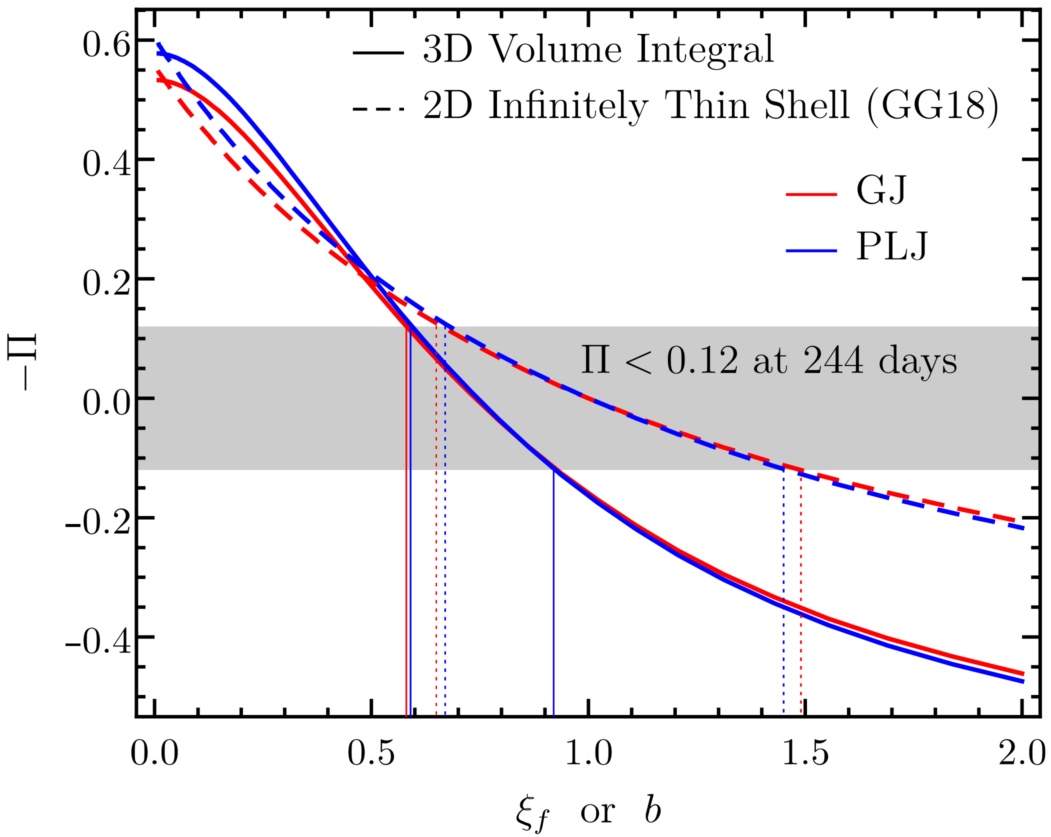

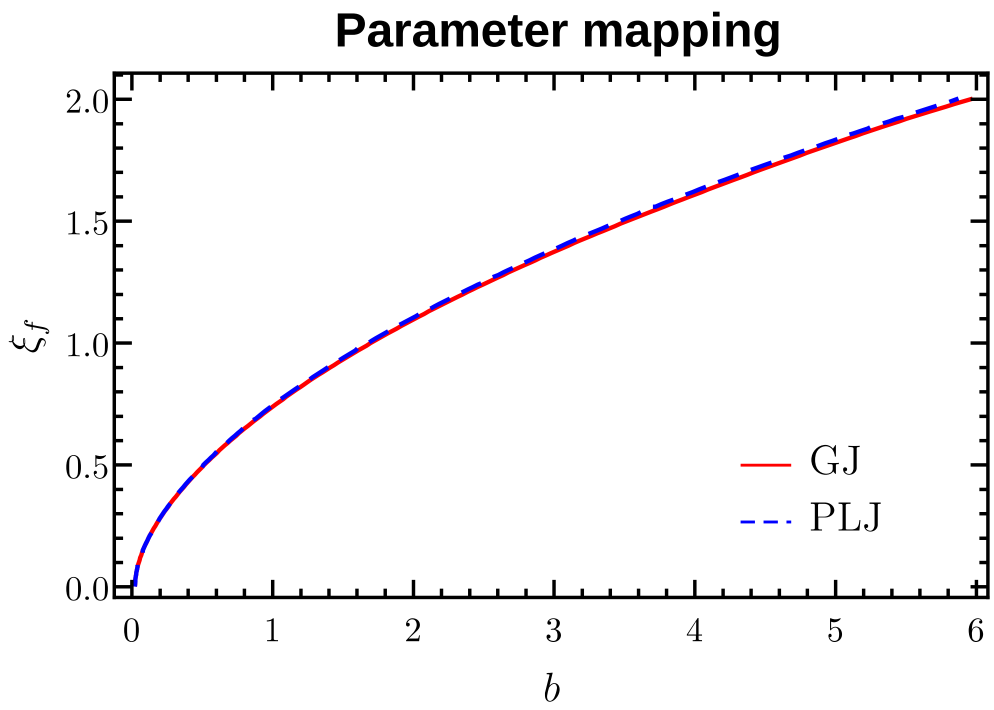

$0.6 \lesssim \xi_f \lesssim 0.9$

(Gill & Granot, in prep)

Flux centroid motion

- Even if the image is unresolved at late times, the flux centroid can yield useful information about the outflow structure.

- Flux centroid motion has been measured from radio observations (Mooley+18):

$$\theta_{\rm fc} = 2.7 \pm 0.3 \text{ mas} \quad (75 \text{ d} - 230 \text{ d})$$

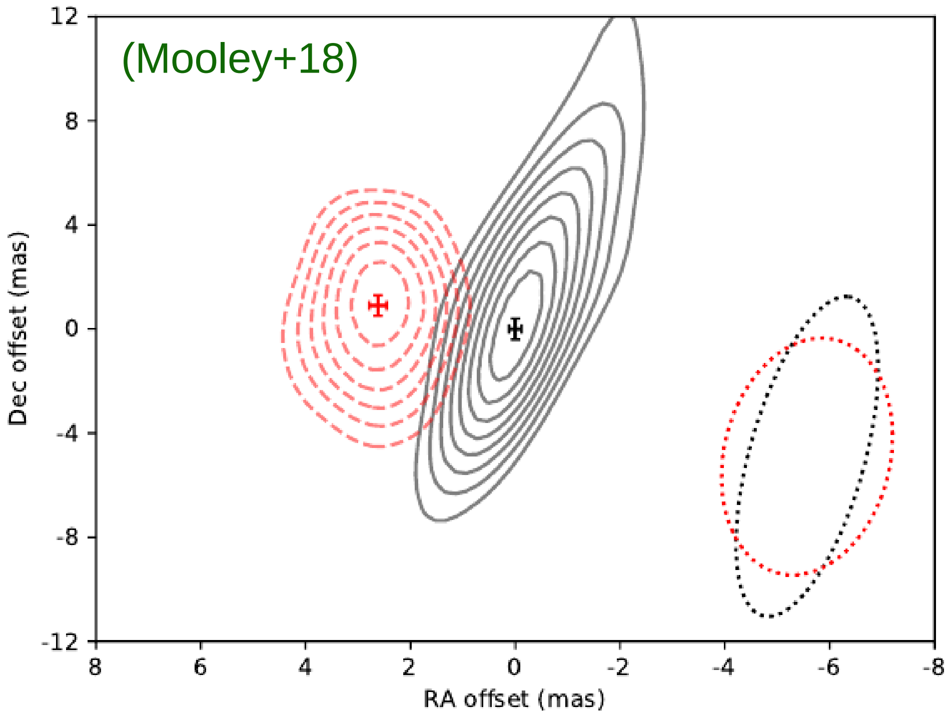

(Gill & Granot 18)

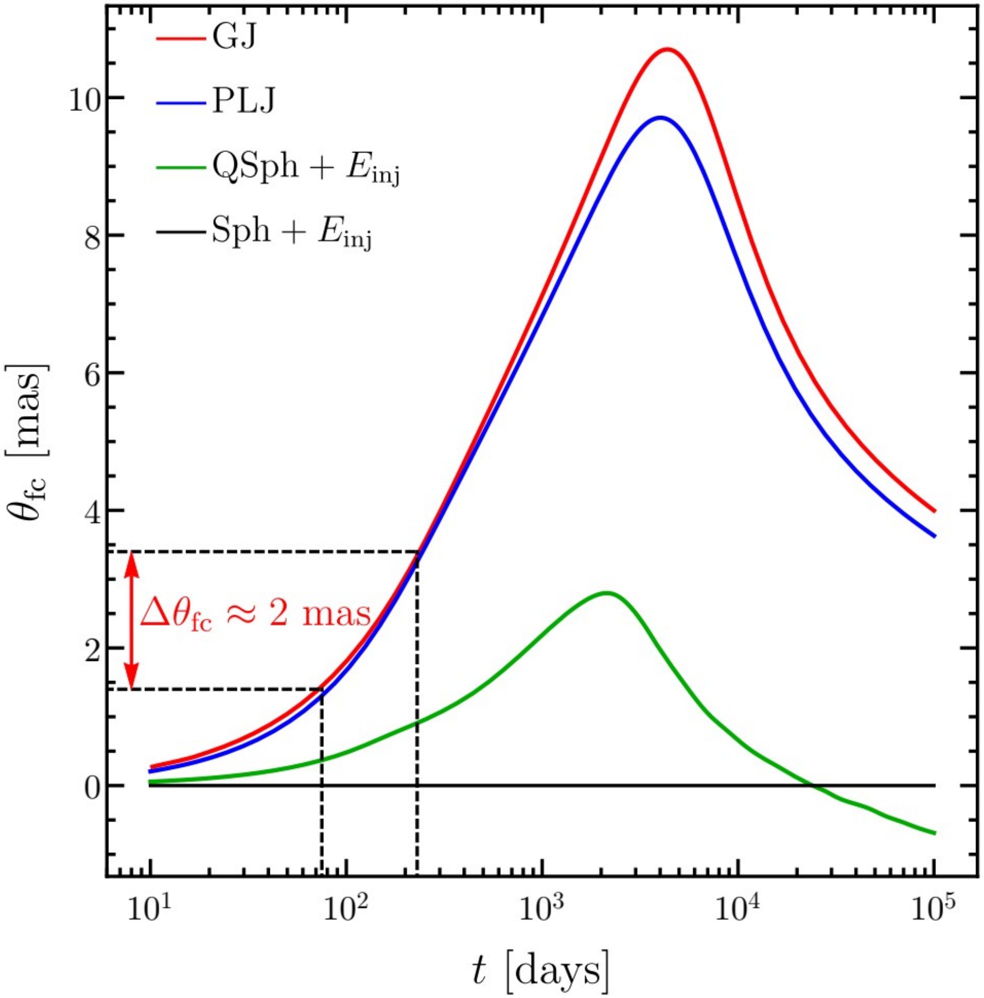

- Apparent superluminal motion

$$v_{\rm app} = (4.1 \pm 0.5)c$$

Image size

- The mean image size may not be a good discriminator between models.
- Structured jets show a larger axial ratio as compared to quasi-spherical outflow models

(Ghirlanda+18)

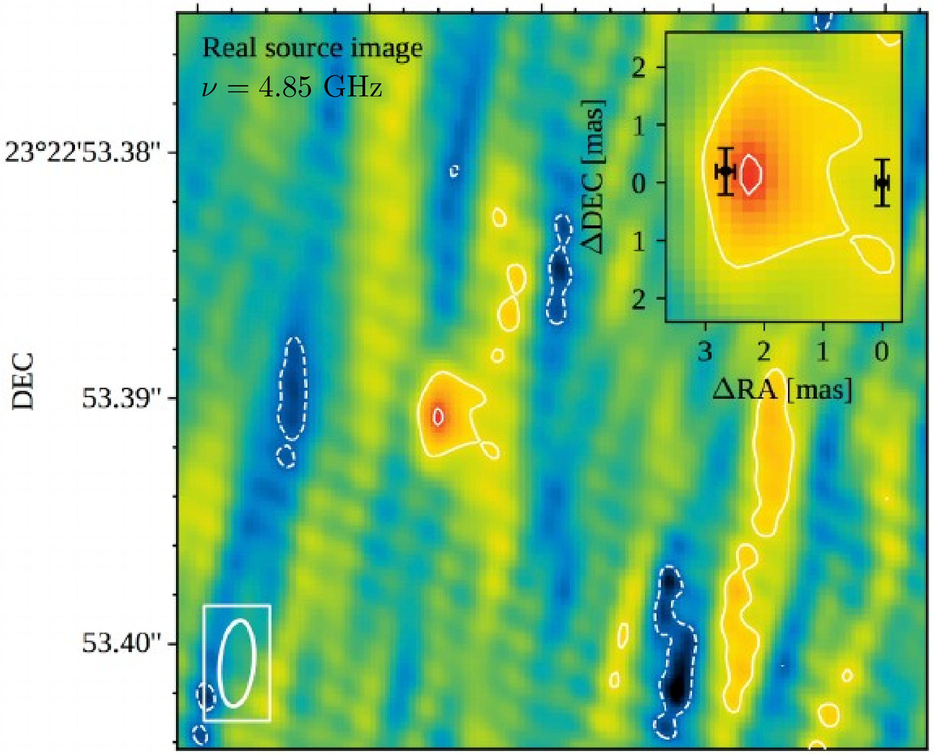

(Gill & Granot 18)

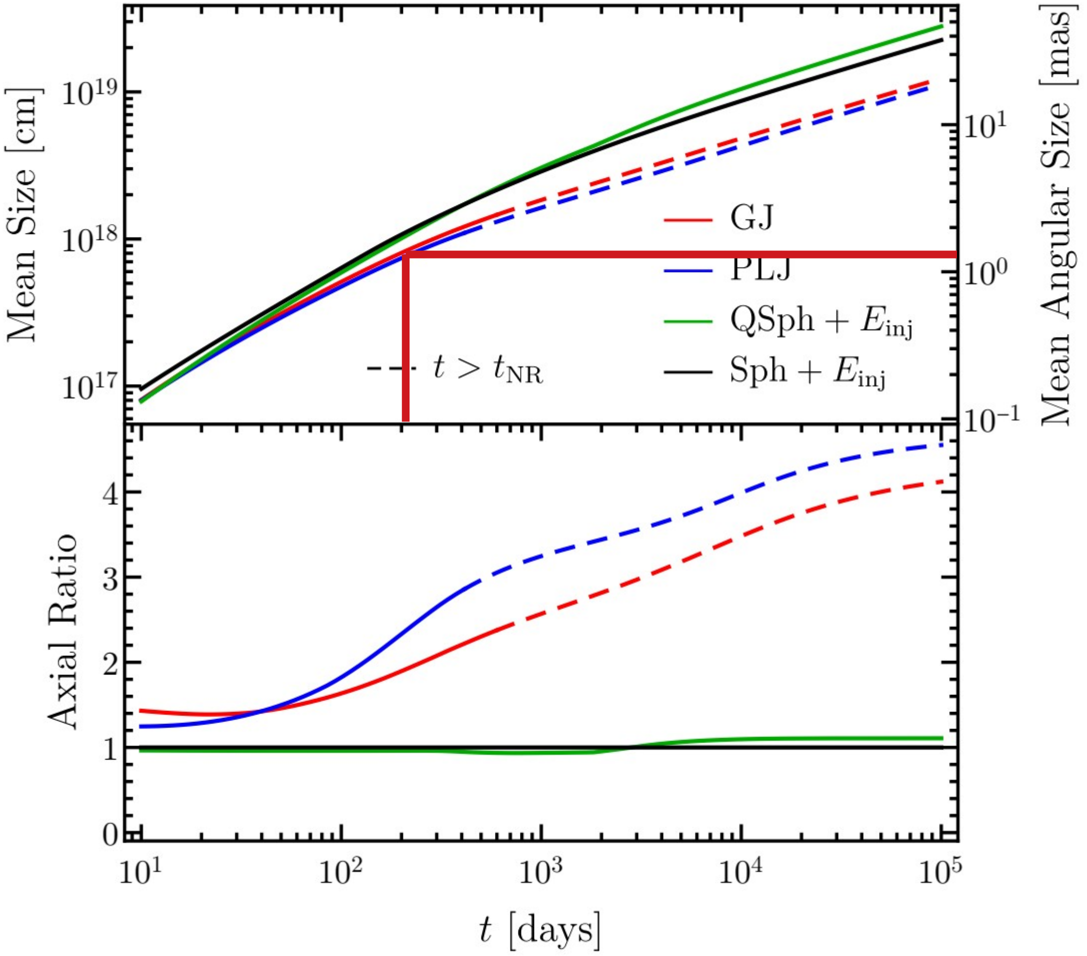

Conclusions

- The total mass of the remnant and kilonova observations suggest that the remnant was a hypermassive NS. The total mass of the blue kilonova ejecta and the delay between the GW chirp signal and the prompt gamma-ray onset suggest that the HMNS survived for about 1 s.

- An initially top-hat jet can explain the afterglow lightcurve and image properties near and after the lightcurve peak when the core of the jet is visible to an off-axis observer.

- Semi-analytic models of structured flows are a useful tool to understand the afterglow lightcurve and image properties. However, improved analytic approaches are needed to capture the dynamics of the flow in the trans-relativistic regime.

- The shallow rise in the afterglow of GRB 170817 before the lightcurve peak (~150 d) can be explained by both a wide-angle quasi-spherical flow and a structured jet. The differences between the two models become apparent after the lightcurve peak.

- The three diagnostics – linear polarization, flux centroid motion, and image size & axial ratio will be useful in distinguishing the properties of the flow in future events.

- Linear polarization upper limit of 12% for GW170817 can be used to constrain the anisotropic structure of the postshock magnetic field.